

Some Aspects of Entanglement Wedge Cross-Section

Komeil Babaei Velni^{*}, M. Reza Mohammadi Mozaffar^{*,†} and M. H. Vahidinia^{‡,†}

^{*} *Department of Physics, University of Guilan, P.O. Box 41335-1914, Rasht, Iran*

[†] *School of Physics, Institute for Research in Fundamental Sciences (IPM),
P.O. Box 19395-5531, Tehran, Iran*

[‡] *Department of Physics, Institute for Advanced Studies in Basic Sciences (IASBS),
P.O. Box 45137-66731, Zanjan, Iran*

E-mails: babaeivelni@guilan.ac.ir, mmohammadi@guilan.ac.ir, vahidinia@iasbs.ac.ir

Abstract

We consider the minimal area of the entanglement wedge cross section (EWCS) in Einstein gravity. In the context of holography, it is proposed that this quantity is dual to different information measures, e.g., entanglement of purification, logarithmic negativity and reflected entropy. Motivated by these proposals, we examine in detail the low and high temperature corrections to this quantity and show that it obeys the area law even in the finite temperature. We also study EWCS in nonrelativistic field theories with nontrivial Lifshitz and hyperscaling violating exponents. The resultant EWCS is an increasing function of the dynamical exponent due to the enhancement of spatial correlations between subregions for larger values of z . We find that EWCS is monotonically decreasing as the hyperscaling violating exponent increases. We also obtain this quantity for an entangling region with singular boundary in a three dimensional field theory and find a universal contribution where the coefficient depends on the central charge. Finally, we verify that for higher dimensional singular regions the corresponding EWCS obeys the area law.

Contents

1	Introduction	1
2	EWCS at Finite Temperature in Relativistic Theories	4
2.1	Low and High Temperature Behavior of HEE and HMI	5
2.1.1	HEE and HMI in $d = 1$	6
2.1.2	HEE and HMI in $d > 1$	7
2.2	Low and High Temperature Behavior of EWCS	10
2.2.1	EWCS in $d = 1$	10
2.2.2	EWCS in $d > 1$	11
3	EWCS in Theories with Lifshitz Scaling and Hyperscaling Violation	13
3.1	Low and High Temperature Behavior of EWCS	14
4	Corner Contributions to EWCS	17
4.1	EWCS for a Union of Kinks in AdS_4	18
4.2	EWCS for a Union of Creases in AdS_{d+2}	20
5	Conclusions and Discussions	22
A	Thermal Corrections to HEE and HMI in Nonrelativistic Theories	23

1 Introduction

In recent years, the study of quantum information concepts such as entanglement using gauge/gravity correspondence has been an active area of research. In particular, improving the duality by adding an explicit relation between a measure of entanglement in the boundary theory and a geometric entity which lives in the bulk spacetime is of great interest. In this context, the Ryu-Takayanagi (RT) proposal is a remarkably simple prescription to compute entanglement entropy (EE) for the QFTs dual to Einstein gravity. Consider a spatial region A in the boundary field theory, the corresponding entanglement entropy between A and its complement is given by [1]

$$S_A = \frac{\text{area}(\Gamma_A)}{4G_N}, \tag{1.1}$$

where G_N is the Newton constant and Γ_A is a codimension-2, spacelike minimal hypersurface in the bulk spacetime, anchored to the asymptotic boundary such that $\partial\Gamma_A = \partial A$ (see figure 1). The RT proposal which passes a variety of consistency tests, generalizes to time dependent case [2] and higher derivative theories of gravity [3–6]. Using these prescriptions, the correlation of several disconnected components can also be considered. In particular when the entangling region is made by two disjoint spatial components, an important quantity to study is the holographic mutual

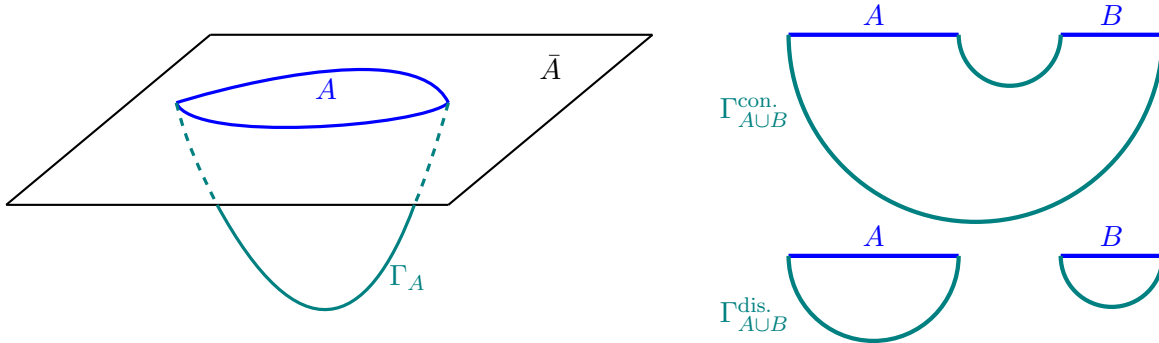


Figure 1: Schematic configurations for computing S_A (left) and S_{AUB} (right). Note that in the latter case we have two different extremal configurations denoted by $\Gamma_{AUB}^{\text{con.}}$ and $\Gamma_{AUB}^{\text{dis.}}$ corresponding to connected and disconnected RT surfaces respectively.

information (HMI) given as follows¹

$$I(A, B) = S_A + S_B - S_{AUB}. \quad (1.2)$$

The mutual information is free from UV divergences and subadditivity guarantees that $I(A, B) \geq 0$. In [7] it was shown that HMI exhibits a phase transition which is due to the competition between two different configurations for computing S_{AB} . Indeed, in order to find this contribution we should consider two minima corresponding to a connected configuration and to a disconnected one (see figure 1). At small distances the connected configuration has the minimal area, while for large separations the RT surface changes topology and the disconnected configuration is favored. Hence using eq.(1.2) the HMI vanishes in the latter case. It is worth to mention that HMI phase transition is a feature of large N limit of quantum field theory and considering $\mathcal{O}(\frac{1}{N})$ corrections changes this picture [8]. Besides the already mentioned case of the HEE and HMI, there are many attempts to construct a holographic prescription for other information measures, e.g., relative entropy [9], quantum information metric [10] and computational complexity [11, 12]. However, in this paper, we focus on another concept that has recently entered this discussion which is the minimal area of the entanglement wedge cross section (EWCS) and on its conjectured holographic duals [13–17]. Given a particular spatial region composed of two components A and B in the boundary theory, the EWCS is given as follows²

$$E_W(\rho_{AB}) = \frac{\text{area}(\Sigma_{AB}^{\text{min}})}{4G_N}, \quad (1.3)$$

where Σ_{AB}^{min} is the minimal cross sectional area of the corresponding entanglement wedge (see Fig.2). Let us now briefly mention different holographic interpretation of this object.

EWCS was proposed by [13, 14] to be dual to the entanglement of purification (EoP), but there

¹In the following we denote S_{AUB} by S_{AB} .

²In the following E_W is used interchangeably with EWCS.

is no proof and the conjecture is mainly based on some properties that EoP should satisfy. Using the entanglement negativity in quantum error-correcting codes and tensor network models of holography, another proposal has been made for E_W in [15]. The authors of this paper identified properties of EWCS with entanglement negativity in holographic theories and made explicit comparisons between E_W and entanglement negativity in a 2-dimensional CFT. Also recently another interpretation of EWCS is given in [17] where the authors show that the entanglement entropy associated to a canonical purification is captured by E_W . They call this quantity the reflected entropy, i.e., S_R , which is a measure of quantum and classical correlations between A and B .

In the following we will focus on the first proposal given in [13, 14] which gives entanglement of purification in terms of E_W . Consider a bipartite system with Hilbert space equal to the direct product of two factors, i.e., $\mathcal{H} = \mathcal{H}_A \otimes \mathcal{H}_B$ and let ρ_{AB} be a density matrix corresponding to a mixed state on \mathcal{H} . It is a well known fact that by adding auxiliary degrees of freedom to \mathcal{H} one can construct a pure state $|\psi\rangle$ out of ρ_{AB} such that $\rho_{AB} = \text{tr}_{A'B'}|\psi\rangle\langle\psi|$ and $|\psi\rangle \in \mathcal{H}_{AA'} \otimes \mathcal{H}_{BB'}$. Indeed, this procedure is not unique and one can find different purifications for a given mixed state. Now following [18], the EoP is defined as

$$E_P(\rho_{AB}) = \min_{\rho_{AB} = \text{tr}_{A'B'}|\psi\rangle\langle\psi|} S_{\rho_{AA'}}, \quad (1.4)$$

where $\rho_{AA'} = \text{tr}_{BB'}|\psi\rangle\langle\psi|$ and the minimization is taken over any $|\psi\rangle$. The EoP is a measure of correlation between A and B and reduces to EE for pure states. Considering a general quantum system, the EoP is subject to the following inequalities³

$$\begin{aligned} \frac{I(A, B)}{2} &\leq E_P(\rho_{AB}) \leq \min(S_A, S_B), \\ E_P(\rho_{A(BC)}) &\geq \frac{I(A, B)}{2} + \frac{I(A, C)}{2}. \end{aligned} \quad (1.5)$$

Based on [13, 14] the holographic EoP of the boundary field theory is given by $E_P(\rho_{AB}) = E_W(\rho_{AB})$. Using this prescription, it was shown that, the resultant quantity obeys all the properties of EoP. Also it was shown that, keeping the geometry of A and B fixed while their separation increases, the holographic EoP has a phase transition such that $E_P = 0$ when the two regions are distant enough. This behavior which is similar to the phase transition of HMI is due to the competition between two different configurations for the entanglement wedge. Despite the fact that in large distance limit, HMI vanishes continuously, the EoP experiences a discontinuous transition. In [20], EoP for a 2-dimensional scalar theory was studied where its behavior qualitatively agrees with the conjectured holographic proposal. Also using a generalization of the above proposal to time dependent backgrounds, [14, 21] studied the evolution of EoP after a quantum quench in the dual field theory. Related investigations attempting to better understand EoP both in the field theory and holography have also appeared in [22–32].

The aim of this paper is to more investigate the holographic aspects of EWCS in field theories

³For a complete set of inequalities see [18, 19] and appendix A of [14].

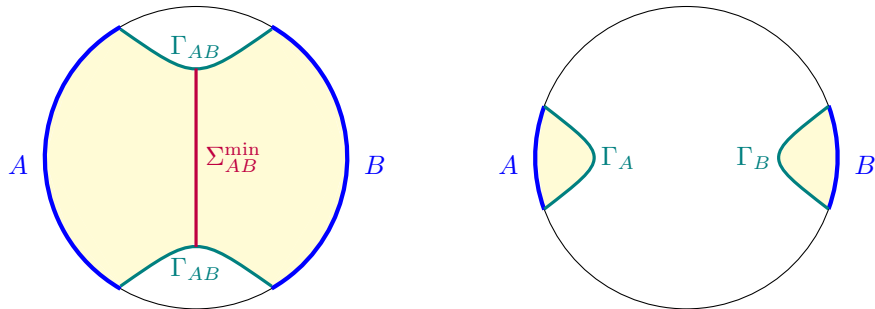


Figure 2: *Left*: Schematic configuration for computing E_W where the entanglement wedge (shaded region) is connected. In this case E_W is proportional to the area of Σ_{AB}^{\min} . *Right*: For small entangling regions where the entanglement wedge is disconnected and Σ_{AB}^{\min} becomes empty the corresponding E_W vanishes.

dual to Einstein gravity. We will study the phase transition of EWCS in a relativistic theory at finite temperature and find the low and high temperature expansion of this quantity. We show explicitly that EWCS obeys an area law scaling even in finite temperature. We also study the transition of EWCS in a non-relativistic QFT with nontrivial dynamical and hyperscaling violating exponents, i.e., z and θ . Moreover, we investigate the properties of EWCS for nonsmooth entangling regions where the boundary contains conical singularity. Considering a simple configuration for the subregions, we find a universal contribution to EWCS due to the presence of corner in a four dimensional field theory when the subregions coincide.

This paper is organized as follows. In section 2, after a short review on HEE and HMI for a strip entangling region at finite temperature, we investigate the corresponding EWCS in different dimensions and obtain analytical results at low and high temperature limits. The role of dynamical and hyperscaling violating exponents in the phase transition of EWCS is discussed in section 3. In section 4, we study the corner contributions to EWCS considering a union of kinks and creases in four and higher dimensions. We conclude with a discussion of our results, as well as possible future directions, in section 5. We relegate some details of the computations to the appendix.

2 EWCS at Finite Temperature in Relativistic Theories

In this section we study the finite temperature contribution to the E_W for holographic theories dual to Einstein gravity. We begin by reviewing the calculation of the finite temperature corrections to HEE and HMI using a systematic expansion, which was originally performed in [33, 34].⁴ Then applying this method allows us to evaluate the thermal corrections to E_W for a straight belt entangling region in section 2.2.

⁴On the CFT side thermal corrections to EE is computed in [35, 36].

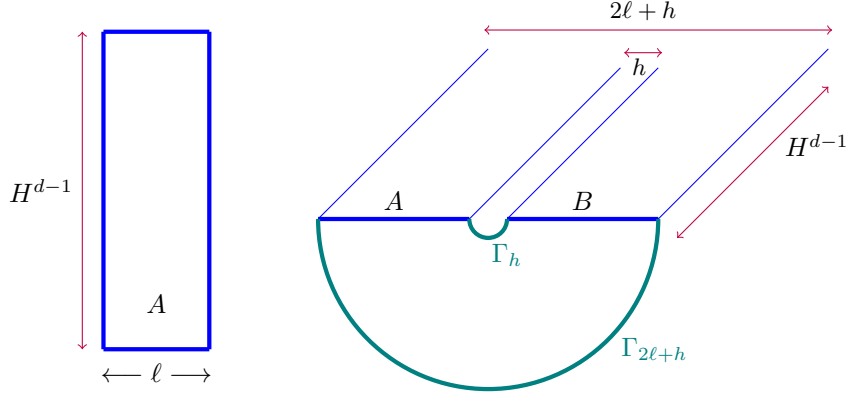


Figure 3: Schematic configuration for computing HEE (left) and HMI (right). In the latter case, we just demonstrate the connected configuration where the HMI is non-zero.

The bulk geometry will be a $(d + 2)$ -dimensional AdS black brane in Poincare coordinates

$$ds^2 = \frac{L^2}{r^2} \left(-f(r)dt^2 + \frac{dr^2}{f(r)} + d\vec{x}^2 \right), \quad f(r) = 1 - \frac{r^{d+1}}{r_0^{d+1}}, \quad (2.1)$$

where r_0 is the horizon radius and L is the AdS radius. In the following without loss of generality we set $L = 1$. From eq.(2.1), one obtains that the temperature and thermal entropy density are given by

$$T = \frac{d+1}{4\pi r_0}, \quad s_{\text{th}} = \frac{1}{4G_N} \frac{1}{r_0^d}. \quad (2.2)$$

Figure 3 shows the entangling regions that we consider for computing HEE and HMI. The straight belt entangling region can be parametrized as

$$-\frac{\ell}{2} \leq x_1(r) \equiv x(r) \leq \frac{\ell}{2}, \quad -\frac{H}{2} \leq x_i \leq \frac{H}{2}, \quad i = 2, \dots, d, \quad (2.3)$$

where we assume $H \gg \ell$.

2.1 Low and High Temperature Behavior of HEE and HMI

In this section we review the computation of HEE for strip entangling region in the low and high temperature limit. This analysis has been done in [33] for HEE and generalized to HMI in [34]. Here we present the main steps and fix our notations.⁵

Employing the RT prescription and using eq.(2.1), the corresponding HEE functional is given

⁵The following analysis does not apply to three dimensional bulk geometry, i.e., $d = 1$. We will come back to this case in section 2.2.1.

by

$$S = \frac{H^{d-1}}{4G_N} \int \frac{dr}{r^d} \sqrt{\frac{1}{f(r)} + x'(r)^2}. \quad (2.4)$$

Extremizing the above expression yields the equation of motion for $x(r)$, however, since there is no explicit $x(r)$ dependence, the corresponding momentum is a conserved quantity. Therefore we find the following first integral

$$x'(r) = \pm \frac{1}{\sqrt{f(r) \left(\left(\frac{r_t}{r} \right)^{2d} - 1 \right)}}, \quad (2.5)$$

where r_t is the turning point of the minimal hypersurface. Using the above expression the relation between ℓ and r_t is given by

$$\ell = 2r_t \int_0^1 \frac{u^d du}{\sqrt{1-u^{2d}}} \left(1 - \left(\frac{r_t}{r_0} \right)^{d+1} u^{d+1} \right)^{-\frac{1}{2}}. \quad (2.6)$$

On the other hand plugging eq.(2.5) back into eq.(2.4), we find

$$S = \frac{1}{2G_N} \frac{H^{d-1}}{r_t^{d-1}} \int_{\frac{\epsilon}{r_t}}^1 \frac{du}{u^d \sqrt{1-u^{2d}}} \left(1 - \left(\frac{r_t}{r_0} \right)^{d+1} u^{d+1} \right)^{-\frac{1}{2}}. \quad (2.7)$$

The above integrals can be carried out analytically in $d = 1$ case. Hence before going to general dimensions, let us first consider this special case which corresponds to a three dimensional bulk geometry.

2.1.1 HEE and HMI in $d = 1$

For $d = 1$ the minimal surface is a spacelike geodesic whose length can be expressed analytically in closed form [37], which enables us to directly extract its temperature behavior in various regimes. In this case eqs.(2.6) and (2.7) become

$$\ell = 2r_t \int_0^1 \frac{u du}{\sqrt{1-u^2}} \left(1 - \left(\frac{r_t}{r_0} \right)^2 u^2 \right)^{-\frac{1}{2}}, \quad S = \frac{1}{2G_N} \int_{\frac{\epsilon}{r_t}}^1 \frac{du}{u \sqrt{1-u^2}} \left(1 - \left(\frac{r_t}{r_0} \right)^2 u^2 \right)^{-\frac{1}{2}}. \quad (2.8)$$

It is straightforward to evaluate these quantities and to produce the result

$$\ell = r_0 \log \frac{r_0 + r_t}{r_0 - r_t}, \quad S = \frac{c}{3} \log \left(\frac{1}{\pi \epsilon T} \sinh \pi \ell T \right), \quad (2.9)$$

where $c = \frac{3}{2G_N}$ denotes the central charge of dual two dimensional CFT. We can make use of the above expression to find the low and high temperature behavior of HEE as follows

$$S \sim S_{\text{div.}} + \begin{cases} \frac{c}{18}(\pi\ell T)^2 + \dots & \ell T \ll 1 \\ \frac{c}{3}\pi\ell T + \dots & \ell T \gg 1 \end{cases}. \quad (2.10)$$

This shows that the thermal fluctuations increases HEE, as expected. In particular, in high temperature limit the leading finite term in HEE takes precisely the form expected for the volume law contribution to the entanglement entropy in the dual field theory due to thermal fluctuations. That is, the leading thermal contribution is proportional to ℓ .

In order to investigate the low and high temperature behavior of HMI, one should keep in mind that we have three different scales, i.e., h , ℓ and T . Considering low temperature with respect to the subregion sizes and the separation between them corresponds to $hT \ll \ell T \ll 1$. One might also regard the $hT \ll 1 \ll \ell T$ case where we only have low temperature with respect to the separation scale. As demonstrated in [34] these two different limits contain distinct physics. Further, in the following we are only interested in cases where HMI is non-zero so we neglect the $hT \gg \ell T$ or $1 \ll hT \ll \ell T$ cases which correspond to disconnected configurations for RT surfaces with zero HMI. For the connected configuration eq.(1.2) becomes

$$I = 2S(\ell) - S(h) - S(2\ell + h). \quad (2.11)$$

Using eq.(2.9) evaluating the above expression is a straightforward exercise, which yields

$$I = \frac{c}{3} \log \frac{\sinh^2(\pi\ell T)}{\sinh(\pi hT) \sinh(\pi(2\ell + h)T)}. \quad (2.12)$$

Equipped with the above result we can compute HMI in different scaling regimes as follows

$$I \sim \frac{c}{3} \begin{cases} \log \frac{\ell}{2h} - \frac{1}{3}(\pi\ell T)^2 + \dots & hT \ll \ell T \ll 1 \\ -\log(2\pi hT) - \pi hT + \log \tanh(\pi\ell T) + \dots & hT \ll 1 \ll \ell T \end{cases}, \quad (2.13)$$

which demonstrates that HMI is a monotonically decreasing function of temperature. Taking the limit for adjacent subregions $h \rightarrow 0$ in the above result, we see that the HMI diverges.

2.1.2 HEE and HMI in $d > 1$

While the integral in eqs.(2.6) and (2.7) cannot be carried out analytically for general $d > 1$, to perform an exact estimation, we employ a particular series expansion which is enough to extract the main behavior of HEE at finite temperature. Using this expansion eq.(2.6) can be written as follows (see [33] for details)

$$\ell = 2r_t \sum_{n=0}^{\infty} \frac{1}{1 + n(d+1)} \frac{\Gamma(n + \frac{1}{2})}{\Gamma(n+1)} \frac{\Gamma\left(\frac{(d+1)(n+1)}{2d}\right)}{\Gamma\left(\frac{(d+1)n+1}{2d}\right)} \left(\frac{r_t}{r_0}\right)^{n(d+1)}, \quad (2.14)$$

which converges for $r_t < r_0$. On the other hand using similar expansion in eq.(2.7), we find

$$S = \frac{1}{2(d-1)G_N} \left(\frac{H}{\epsilon} \right)^{d-1} + S_{\text{finite.}}, \quad (2.15)$$

where

$$S_{\text{finite.}} = \frac{1}{4G_N} \frac{H^{d-1}}{r_t^{d-1}} \left(\frac{c}{1-d} + \sum_{n=1}^{\infty} \frac{1}{d} \frac{\Gamma(n + \frac{1}{2})}{\Gamma(n+1)} \frac{\Gamma\left(\frac{n(d+1)-d+1}{2d}\right)}{\Gamma\left(\frac{n(d+1)+1}{2d}\right)} \left(\frac{r_t}{r_0}\right)^{n(d+1)} \right), \quad (2.16)$$

and we have define $c = \frac{2\sqrt{\pi}\Gamma\left(\frac{d+1}{2d}\right)}{\Gamma\left(\frac{1}{2d}\right)}$. Now it is straightforward to find the low and high temperature behavior of HEE using eqs. (2.14) and (2.16).

(i) HEE at Low Temperature Limit $\ell T \ll 1$

In this case using eq.(2.2) the $\ell T \ll 1$ limit can be interpreted in terms of bulk data as $r_t \ll r_0$. In this limit eq.(2.14) yields

$$r_t = \frac{\ell}{c} \left(1 - \frac{\sqrt{\pi}}{(d+2)c^{d+2}} \frac{\Gamma\left(\frac{d+1}{d}\right)}{\Gamma\left(\frac{d+2}{2d}\right)} \left(\frac{\ell}{r_0}\right)^{d+1} + \mathcal{O}\left(\left(\frac{\ell}{r_0}\right)^{2(d+1)}\right) \right). \quad (2.17)$$

Substituting the above expression into eq.(2.16) and expand to leading order in the temperature, we finally obtain

$$S_{\text{finite.}} = \frac{\mathcal{C}_0}{4G_N} \frac{H^{d-1}}{\ell^{d-1}} \left(1 + \mathcal{C}_1(\ell T)^{d+1} + \mathcal{O}((\ell T)^{2(d+1)}) \right), \quad (2.18)$$

where

$$\mathcal{C}_0 = \frac{c^d}{1-d}, \quad \mathcal{C}_1 = \left(\frac{4\pi}{d+1} \right)^{d+1} \frac{\sqrt{\pi}}{2c^{d+2}} \frac{1-d}{d+2} \frac{\Gamma\left(\frac{1}{d}\right)}{\Gamma\left(\frac{d+2}{2d}\right)}. \quad (2.19)$$

According to eq.(2.18), the thermal fluctuations increases the HEE, as expected (note that \mathcal{C}_0 and \mathcal{C}_1 are both negative).

(ii) HEE at High Temperature Limit $\ell T \gg 1$

As the length of the subregion becomes large, the turning point of the corresponding hypersurface approaches the horizon and eventually, the minimal hypersurface covers a part of the horizon. In this case the entanglement entropy is determined entirely by the contributions coming from the near horizon part of the minimal hypersurface [37]. Hence we must consider eqs.(2.14) and (2.16)

in the limit that $r_t \rightarrow r_0$. After some algebra, eq.(2.16) becomes

$$S_{\text{finite}} = \frac{H^{d-1}}{4G_N r_t^{d-1}} \left(\frac{\ell}{r_t} - \frac{dc}{d-1} + \sum_{n=1}^{\infty} \frac{2d}{n(d+1)+1-d} \frac{1}{n(d+1)+1} \frac{\Gamma(n+\frac{1}{2})}{\Gamma(n+1)} \frac{\Gamma\left(\frac{(d+1)(n+1)}{2d}\right)}{\Gamma\left(\frac{n(d+1)+1}{2d}\right)} \left(\frac{r_t}{r_0}\right)^{n(d+1)} \right).$$

It is easy to see that in the large n limit the above infinite series behaves as $\frac{1}{n^2} \left(\frac{r_t}{r_0}\right)^{n(d+1)}$, so we can safely consider $r_t \rightarrow r_0$ limit. Hence the final result for the finite part of the HEE in this case becomes

$$S_{\text{finite}} = \frac{\ell H^{d-1}}{4G_N} \left(\frac{4\pi T}{d+1} \right)^d \left(1 + \frac{d+1}{4\pi\ell T} \mathcal{C}_2 \right), \quad (2.20)$$

where

$$\mathcal{C}_2 = -\frac{dc}{d-1} + 2 \sum_{n=1}^{\infty} \frac{d}{n(d+1)+1-d} \frac{1}{n(d+1)+1} \frac{\Gamma(n+\frac{1}{2})}{\Gamma(n+1)} \frac{\Gamma\left(\frac{(d+1)(n+1)}{2d}\right)}{\Gamma\left(\frac{n(d+1)+1}{2d}\right)}. \quad (2.21)$$

Note that the first term in eq.(2.20) shows a volume law which is a typical property of entanglement entropy at finite temperature and shows that for a mixed thermal state EE measures both classical and quantum correlations.

(iii) HMI at Low and High Temperature Limit

Now we are equipped with all we need to calculate the HMI for configuration depicted in figure 3 using eqs. (2.18) and (2.20). As we mentioned before, we are only interested in cases where the HMI is non-zero corresponding to a connected configuration. In this case using eqs. (1.2) and (2.15), we have

$$I = 2S_{\text{finite.}}(\ell) - S_{\text{finite.}}(h) - S_{\text{finite.}}(2\ell + h). \quad (2.22)$$

Considering the $hT \ll \ell T \ll 1$ limit and using eq.(2.18) for all three distinct entropies appear in the above expression, yields [34, 38]

$$I = I_{T=0} - C_0 C_1 \frac{H^{d-1}}{2G_N} (\ell + h)^2 T^{d+1}, \quad (2.23)$$

where $I_{T=0}$ is the HMI at zero temperature, which in this case is given by

$$I_{T=0} = C_0 \frac{H^{d-1}}{4G_N} \left(\frac{2}{\ell^{d-1}} - \frac{1}{h^{d-1}} - \frac{1}{(2\ell + h)^{d-1}} \right). \quad (2.24)$$

We note again that the finite temperature corrections reduce the HMI so the mutual correlations between subregions decrease. Another interesting case to consider is $hT \ll 1 \ll \ell T$, for which using

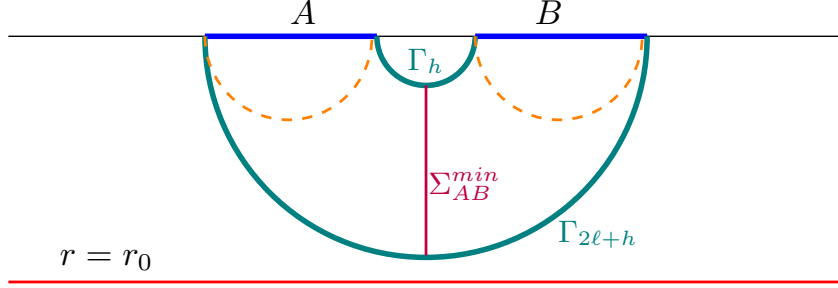


Figure 4: Schematic configuration for computing $E_W(\rho_{AB})$.

eqs. (2.18) and (2.20) we find

$$I = \frac{H^{d-1}T^{d-1}}{4G_N} \left(-\frac{\mathcal{C}_0}{(hT)^{d-1}} + \left(\frac{4\pi}{d+1} \right)^{d-1} \mathcal{C}_2 - \left(\frac{4\pi}{d+1} \right)^d hT - \mathcal{C}_0 \mathcal{C}_1 (hT)^2 \right). \quad (2.25)$$

The second term in the above expression which is proportional to the area of the entangling region shows that the HMI obeys an area law even in finite temperature.

2.2 Low and High Temperature Behavior of EWCS

We turn now to the calculation of E_W , using the recent holographic prescription given in [13, 14]. According to this, the E_W of a certain combined region AB is given by eq.(1.3). Since we focus on the case of two intervals which have a reflection symmetry about $x = 0$, we expect that the corresponding minimal configuration respects this symmetry. Indeed, in this case Σ_{AB}^{\min} runs along the radial direction and connects the corresponding turning points of Γ_h and $\Gamma_{2\ell+h}$ (see Fig.4). Using eq.(2.1), the area of this hypersurface can be written as

$$E_W = \frac{H^{d-1}}{4G_N} \int_{r_t(h)}^{r_t(2\ell+h)} \frac{dr}{r^d \sqrt{1 - \frac{r^{d+1}}{r_0^{d+1}}}}. \quad (2.26)$$

Evaluating the above integral is a straightforward exercise both for $d = 1$ and $d > 1$. Below we consider these cases separately.

2.2.1 EWCS in $d = 1$

In this case where the boundary theory lives in two dimensions, performing the integral in eq.(2.26), we are left with

$$E_W = \frac{1}{4G_N} \log \left(\frac{r_t(2\ell+h)}{r_t(h)} \frac{1 + \sqrt{f(r_t(2\ell+h))}}{1 + \sqrt{f(r_t(h))}} \right). \quad (2.27)$$

Using eq.(2.9), the above expression can be rewritten as follows

$$E_W = \frac{c}{6} \log \frac{\tanh \frac{\pi(2\ell+h)T}{2}}{\tanh \frac{\pi h T}{2}}. \quad (2.28)$$

Hence using the above result we can find EWCS in different scaling regimes. For $hT \ll \ell T \ll 1$ one finds

$$E_W = \frac{c}{6} \log \frac{2\ell}{h} - \frac{c}{18} (\pi \ell T)^2 + \dots, \quad (2.29)$$

where the first term is just the zero temperature E_W . The second term with a negative sign shows that finite temperature reduces E_W and therefore two subsystems becomes more disentangled. On the other hand for $hT \ll 1 \ll \ell T$ we have

$$E_W = -\frac{c}{6} \log \frac{\pi h T}{2} + \frac{c}{6} \log \tanh(\pi \ell T) + \dots, \quad (2.30)$$

where we have neglected terms those suppress exponentially with ℓT . Note that the first inequality in eq.(1.5) satisfied in both low and high temperature limits. Also taking the limit for adjacent subregions $h \rightarrow 0$ in the above result, we see that the EWCS diverges.

The behavior of E_W in a two dimensional field theory can be read off from Fig.5. The left panel shows the two dimensional parameter space restricted by the $E_W \neq 0$ condition. Note that it is convenient to define dimensionless variables hT and $\frac{h}{\ell}$. The nonzero E_W corresponds to the red shaded region where the correlation between two subregions are nonvanishing. According to this plot, keeping the length of A and B fixed while their separation increases, the EWCS shows a discontinuous phase transition, such that $E_W = 0$ when the two regions are distant enough. Further EWCS is a monotonically decreasing function of temperature such that in high temperature limit vanishes. It is worth to mention that precisely, the similar situation arose in [33] where the structure of HMI has been investigated, although the HMI transition is continuous.

2.2.2 EWCS in $d > 1$

In this case the integral in eq.(2.26) can be rewritten as follows⁶

$$\begin{aligned} E_W &= \frac{H^{d-1}}{4G_N} \int_{r_t(h)}^{r_t(2\ell+h)} \frac{dr}{r^d} \sum_{n=0}^{\infty} \frac{\Gamma(n + \frac{1}{2})}{\sqrt{\pi} \Gamma(n+1)} \left(\frac{r}{r_0}\right)^{n(d+1)}, \\ &= \frac{H^{d-1}}{4G_N} \sum_{n=0}^{\infty} \frac{\Gamma(n + \frac{1}{2})}{\sqrt{\pi} \Gamma(n+1)} \frac{1}{r_0^{n(d+1)}} \frac{r_t(2\ell+h)^{n(d+1)-d+1} - r_t(h)^{n(d+1)-d+1}}{n(d+1) - d + 1}. \end{aligned} \quad (2.31)$$

⁶Note that although evaluating this integral gives an exact result [21]

$$E_W = \frac{H^{d-1}}{4(1-d)G_N} \left(\frac{\sqrt{f(r)}}{r^{d-1}} - \frac{d-3}{4} \frac{r^2}{r_0^{d+1}} {}_2F_1 \left(\frac{1}{2}, \frac{2}{d+1}, \frac{d+3}{d+1}, \frac{r^{d+1}}{r_0^{d+1}} \right) \right) \Big|_{r_t h}^{r_t(2\ell+h)},$$

using the systematic expansion method is more tractable to find the low and high temperature corrections of EWCS.

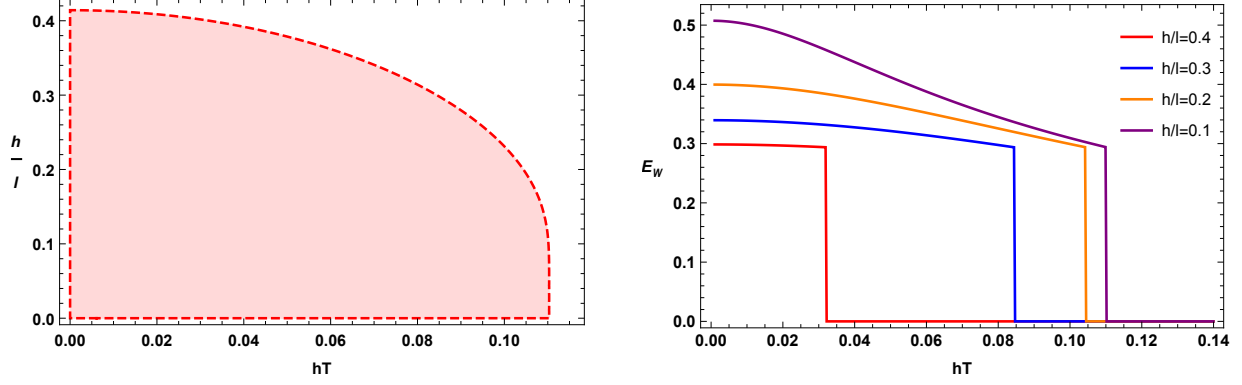


Figure 5: *Left*: parameter space for $d = 1$ where E_W is nonzero only in the red shaded region. *Right*: E_W as a function of hT for different values of h/ℓ . In all these cases E_W undergoes a discontinuous phase transition beyond which it is identically zero. Here we set $c = 1$.

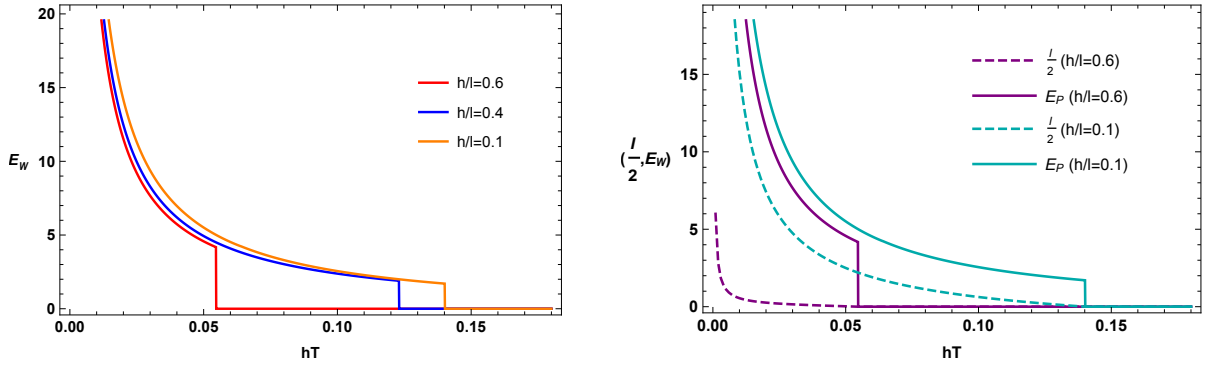


Figure 6: *Left*: E_W as a function of hT for different values of h/ℓ in $d = 2$. In all these cases E_W undergoes a discontinuous phase transition beyond which it is identically zero. *Right*: Checking $I/2 \leq E_W$. Here we set $H/G_N = 1$.

Using this expression one can study the behavior of E_W as a function of h , ℓ and T . While various dimensions do not yield the same results quantitatively, they still agree at a qualitative level. Therefore in the following we focus on $d = 2$ case. The left panel of Fig.6 shows E_W as a function of hT for different values of $\frac{h}{\ell}$. Once again we observe that E_W is a monotonically decreasing function of temperature and vanishes for far away regions. As a consistency check in the right panel we plot both E_W and $\frac{I}{2}$ to see whether eq.(1.5) is satisfied or not.

It is also interesting to look at low and high temperature expansions of E_W . At the low temperature, considering the $hT \ll \ell T \ll 1$ limit and using eq.(2.17) for $r_t(h)$ and $r_t(2\ell + h)$, eq.(2.31) yields

$$E_W = E_W(T = 0) - 2\mathcal{C}_0\mathcal{C}_1 \frac{H^{d-1}}{G_N} \frac{c'}{c} \ell(\ell + h)T^{d+1} + \dots, \quad (2.32)$$

where

$$c' = \frac{1}{d} \left(1 - \frac{\sqrt{\pi} d(d+2)}{2^{1/d}} \frac{\Gamma\left(\frac{d+2}{2d}\right)}{\Gamma\left(\frac{1}{2d}\right)^2} \right), \quad (2.33)$$

and $E_W(T=0)$ is the EWCS at zero temperature, which in this case is given by

$$E_W(T=0) = \frac{C_0}{c} \frac{H^{d-1}}{4G_N} \left(-\frac{1}{h^{d-1}} + \frac{1}{(2\ell+h)^{d-1}} \right). \quad (2.34)$$

On the other hand in $hT \ll 1 \ll \ell T$ limit corresponding to $r_t(h) \ll r_0$ and $r_t(2\ell+h) \rightarrow r_0$ we reexpress eq.(2.31) as follows

$$E_W = \frac{H^{d-1}}{4G_N} \sum_{n=0}^{\infty} \frac{1}{n(d+1)-d+1} \frac{\Gamma\left(n+\frac{1}{2}\right)}{\sqrt{\pi}\Gamma(n+1)} \left(\frac{r_t(2\ell+h)^{n(d+1)-d+1}}{r_0^{n(d+1)}} - \frac{r_t(h)^{n(d+1)-d+1}}{r_0^{n(d+1)}} \right). \quad (2.35)$$

It is easy to see that in the large n limit the first infinite series behaves as $\frac{1}{n^{3/2}} \left(\frac{r_t(2\ell+h)}{r_0} \right)^{n(d+1)}$, so we can safely consider $r_t(2\ell+h) \rightarrow r_0$ limit. Also to consider $r_t(h) \ll r_0$ limit we keep only the leading order terms in the second infinite series, which yields

$$E_W = \frac{H^{d-1} T^{d-1}}{4G_N} \left(-\frac{C_0}{c(hT)^{d-1}} + \left(\frac{4\pi}{d+1} \right)^d C_2' + 2\frac{c'}{c} C_0 C_1 (hT)^2 \right), \quad (2.36)$$

where $C_2' = \frac{\Gamma\left(\frac{1-d}{1+d}\right)}{4\sqrt{\pi}\Gamma\left(\frac{3-d}{2(1+d)}\right)}$. The first term in the above expression diverges in $h \rightarrow 0$ limit where the subregions coincide. Further, the second term which is proportional to the area of the entangling region shows that the EWCS obeys an area law even in finite temperature. As we mentioned before, for a mixed thermal state HEE measures both classical and quantum correlations and as a result scales with the volume. Therefore we may conclude that E_W carries more relevant content than HEE as far as computing quantum entanglement is concerned.

3 EWCS in Theories with Lifshitz Scaling and Hyperscaling Violation

In this section we study the finite temperature contribution to the entanglement wedge cross section in holographic theories with general dynamical critical exponent z and hyperscaling violation exponent θ . These theories admit a fixed point where the system is invariant under the following anisotropic scaling transformation

$$r \rightarrow \lambda r, \quad t \rightarrow \lambda^z t, \quad \vec{x} \rightarrow \lambda \vec{x}, \quad ds \rightarrow \lambda^{\frac{\theta}{d}} ds. \quad (3.1)$$

Various holographic aspects of these theories have been studied in [39–44]. In particular, authors of [34] have studied the HEE and HMI of these theories at finite temperature.⁷ In what follows, similar to section 2, we consider an entangling region in the shape of a strip and calculate finite temperature corrections to EWCS. For completeness, we also briefly review the main result of [34] about HEE and HMI in theories with Lifshitz scaling and hyperscaling violation at the finite temperature in the appendix A.

Let us consider a $(d+2)$ -dimensional black brane solution in the Einstein theory of gravity with appropriate matter field (*e.g.* see [39])

$$ds^2 = \frac{1}{r_f^{2\theta/d}} \frac{1}{r^{2\frac{d-\theta}{d}}} \left(-\frac{f(r)}{r^{2(z-1)}} dt^2 + \frac{dr^2}{f(r)} + d\vec{x}^2 \right), \quad f(r) = 1 - \left(\frac{r}{r_0} \right)^{d-\theta+z}, \quad (3.2)$$

where r_0 is the horizon radius. In addition, r_f is a length scale which fixes the dimensions when $\theta \neq 0$ and in the following without loss of generality we set $r_f = 1$. As mentioned in [39], the null energy condition implies some bounds on values of θ and z

$$(d-\theta)(d(z-1)-\theta) \geq 0, \quad (z-1)(d-\theta+z) \geq 0. \quad (3.3)$$

The temperature and thermal entropy density for eq.(3.2) are given by

$$T = \frac{|d-\theta+z|}{4\pi r_0^z}, \quad s_{\text{th}} = \frac{1}{4G_N} \frac{1}{r_0^{d-\theta}}. \quad (3.4)$$

It is easy to see that the entropy density scales as $s_{\text{th}} \sim T^{\frac{d-\theta}{z}}$. For $z=1$, it shows that hyperscaling violating exponent effectively reduces the dimensionality of the model. As we will see in what follows it is a typical role of θ . The thermodynamic stability of black brane solution requires a positive specific heat which restricts θ and z further

$$\frac{d-\theta}{z} \geq 0. \quad (3.5)$$

In addition, as argued in [39], entanglement entropy analysis at zero temperature as well as string theory realization of hyperscaling violating geometries imply inconsistency when $\theta > d$. So, in what follows we assume $d-\theta > 0$ and $z \geq 1$ which satisfy both eqs. (3.5) and (3.3).

3.1 Low and High Temperature Behavior of EWCS

Now we calculate E_W for holographic theories with hyperscaling violating geometry, using the holographic prescription [13, 14]. The E_W for configuration depicted in Fig.4 for a QFT dual to

⁷It is worth to mention that various aspects of entanglement measures in QFTs with Lifshitz scaling symmetry are studied in [45–48].

eq.(3.2) can be written as

$$E_W = \frac{H^{d-1}}{4G_N} \int_{r_t(h)}^{r_t(2\ell+h)} \frac{dr}{r^{\tilde{d}} \sqrt{1 - \frac{r^{\tilde{d}+z}}{r_0^{\tilde{d}+z}}}}, \quad (3.6)$$

where an effective dimension $\tilde{d} = d - \theta$ is defined. It is easy to see that, for $\theta = d - 1$ and $z = 1$, this expression reduces to what we have obtained for a three dimensional theory in section 2.2.1. Moreover, for $\theta = d$, as eqs.(A.2) and (A.4) show, the RT surface lies on boundary slice $r = \epsilon$ and there is no turning point at all. So, the notion of entangling wedge is not well defined. Indeed, in this case the HEE exhibits an extensive violation of area law [39]. In the rest of this section we neglect these two special cases and calculate the EWCS at low and high temperature limits.

Employing binomial series for the integrand of eq.(2.26), the EWCS integral can be rewritten as follows

$$\begin{aligned} E_W &= \frac{H^{d-1}}{4G_N} \int_{r_t(h)}^{r_t(2\ell+h)} \frac{dr}{r^{\tilde{d}}} \sum_{n=0}^{\infty} \frac{\Gamma(n + \frac{1}{2})}{\sqrt{\pi}\Gamma(n+1)} \left(\frac{r}{r_0}\right)^{n(\tilde{d}+z)}, \\ &= \frac{H^{d-1}}{4G_N} \sum_{n=0}^{\infty} \frac{\Gamma(n + \frac{1}{2})}{\sqrt{\pi}\Gamma(n+1)} \frac{1}{r_0^{n(\tilde{d}+z)}} \frac{r_t(2\ell+h)^{n(\tilde{d}+z)-\tilde{d}+1} - r_t(h)^{n(\tilde{d}+z)-\tilde{d}+1}}{n(\tilde{d}+z) - \tilde{d} + 1}. \end{aligned} \quad (3.7)$$

Let us consider $hT \ll \ell T \ll 1$ limit where we can use eq. (A.8) for $r_t(h)$ and $r_t(2\ell+h)$ to obtain E_W at low temperature limit

$$E_W = E_W(T=0) - \tilde{C}_0 \tilde{C}_1 \frac{H^{d-1}}{2G_N} \frac{\tilde{c}'}{\tilde{c}} ((2\ell+h)^{z+1} - h^{z+1}) T^{\frac{\tilde{d}+z}{z}} + \dots, \quad (3.8)$$

where \tilde{C}_0 and \tilde{C}_1 are defined in eq.(A.10) and

$$\tilde{c}' = \frac{1}{2} \left(\frac{1+z}{\tilde{d}} - \frac{2\Gamma\left(\frac{\tilde{d}+1}{2\tilde{d}}\right)\Gamma\left(\frac{3\tilde{d}+z+1}{2\tilde{d}}\right)}{\Gamma\left(\frac{1}{2\tilde{d}}\right)\Gamma\left(\frac{2\tilde{d}+z+1}{2\tilde{d}}\right)} \right). \quad (3.9)$$

In addition, $E_W(T=0)$ corresponds to EWCS at zero temperature

$$E_W(T=0) = \frac{\tilde{C}_0}{\tilde{c}} \frac{H^{d-1}}{4G_N} \left(-\frac{1}{h^{\tilde{d}-1}} + \frac{1}{(2\ell+h)^{\tilde{d}-1}} \right). \quad (3.10)$$

Considering $z > 1$ and $\tilde{d} > 0$ case, eq.(3.8) shows that E_W decreases with temperature, as expected. In addition, eq.(3.10) shows that with decreasing effective dimension \tilde{d} (θ increasing), E_W decreases. On the other hand in $hT \ll 1 \ll \ell T$ limit corresponding to $r_t(h) \ll r_0$ and $r_t(2\ell+h) \rightarrow r_0$ we

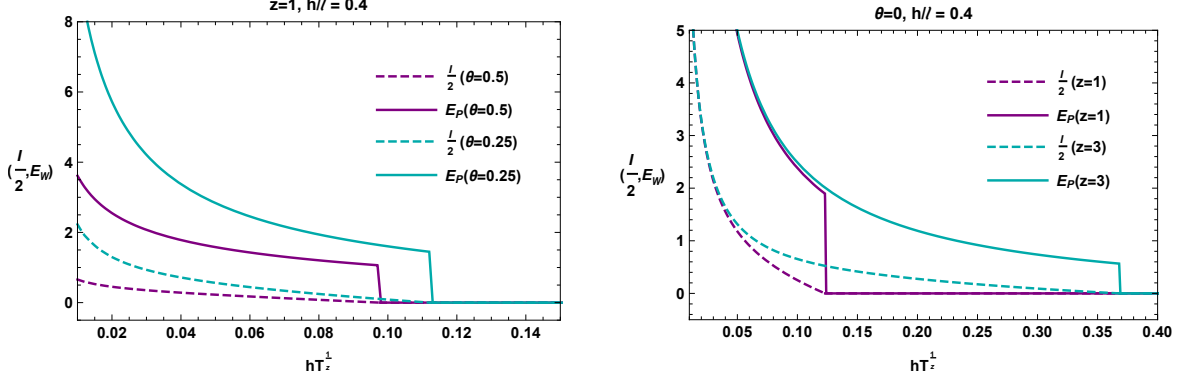


Figure 7: EWCS as a function of $hT^{\frac{1}{2}}$ for different values of z and θ . We also plot $\frac{I}{2}$ to check eq.(1.5). Here we set $H/G_N = 1$ and $d = 2$.

reexpress eq.(3.7) as follows

$$E_W = \frac{H^{d-1}}{4G_N} \sum_{n=0}^{\infty} \frac{1}{n(\tilde{d}+z) - \tilde{d} + 1} \frac{\Gamma(n + \frac{1}{2})}{\sqrt{\pi}\Gamma(n+1)} \left(\frac{r_t(2\ell+h)^{n(\tilde{d}+z)-\tilde{d}+1}}{r_0^{n(\tilde{d}+z)}} - \frac{r_t(h)^{n(\tilde{d}+z)-\tilde{d}+1}}{r_0^{n(\tilde{d}+z)}} \right). \quad (3.11)$$

In the large n limit the first infinite series behaves as $\frac{1}{n^{3/2}} \left(\frac{r_t(2\ell+h)}{r_0} \right)^{n(\tilde{d}+z)}$, so we can safely consider $r_t(2\ell+h) \rightarrow r_0$ limit. Also to consider $r_t(h) \ll r_0$ limit, we keep only the first two terms in the second infinite series, which yields

$$E_W = \frac{H^{d-1}T^{\frac{\tilde{d}-1}{z}}}{4G_N} \left(-\frac{\tilde{C}_0}{\tilde{c}(hT^{\frac{1}{2}})^{\tilde{d}-1}} + \left(\frac{4\pi}{|\tilde{d}+z|} \right)^{\frac{\tilde{d}}{z}} \tilde{C}'_2 + 2\frac{\tilde{c}'}{\tilde{c}} \tilde{C}_0 \tilde{C}_1 (hT^{\frac{1}{2}})^{z+1} \right), \quad (3.12)$$

where

$$\tilde{C}'_2 = \left(\frac{|\tilde{d}+z|}{4\pi} \right)^{\frac{1}{z}} \sum_{n=0}^{\infty} \frac{1}{n(\tilde{d}+z) - \tilde{d} + 1} \frac{\Gamma(n + \frac{1}{2})}{\sqrt{\pi}\Gamma(n+1)} = \frac{1}{1-\tilde{d}} \left(\frac{|\tilde{d}+z|}{4\pi} \right)^{\frac{1}{z}} {}_2F_1 \left(\frac{1}{2}, \frac{1-\tilde{d}}{\tilde{d}+z}, \frac{z+1}{\tilde{d}+z}, 1 \right). \quad (3.13)$$

In Figs.7 and 8 we plot E_W as a function of $hT^{\frac{1}{2}}$ for different values of z and θ . Once again we observe that E_W is a monotonically decreasing function of temperature and vanishes for distant enough regions. As illustrated in these figures, the transition point depends on the value of dynamical and hyperscaling violation exponents. In particular, in Fig.7 we have compared EWCS and HMI for different values of z and θ which in all cases eq.(1.5) satisfied. Based on these figures E_W is an increasing function of the dynamical exponent, i.e., z , and the transition which happens in large separation or high temperature limit is slower in comparing to the relativistic case with $z = 1$. Such a behavior is not surprising because as discussed in [45] the spatial correlations between subregions become stronger for larger values of z . On the other hand as is clear from the graphs, E_W is monotonically decreasing as the hyperscaling violating exponent increases. As we mentioned

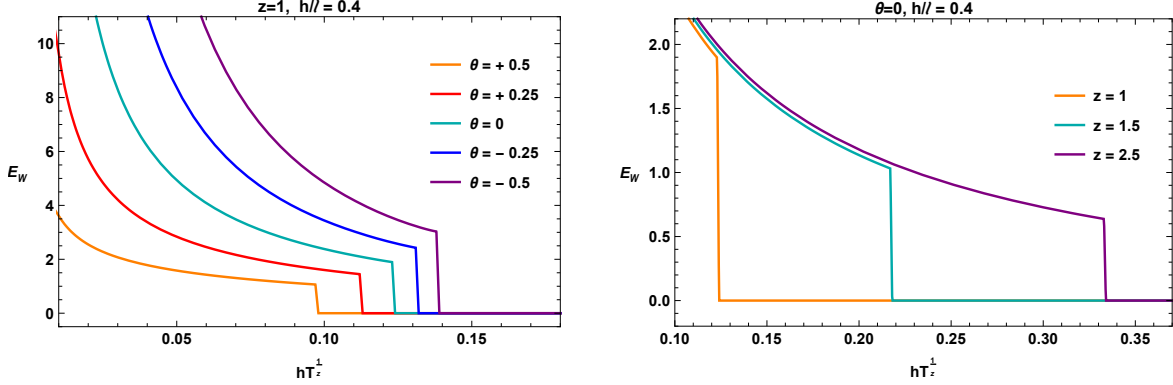


Figure 8: EWCS as a function of $hT^{\frac{1}{z}}$ for different values of θ and z . *Left*: E_W decreases as θ increases. *Right*: E_W increases as z increases. Here we set $H/G_N = 1$ and $d = 2$.

before hyperscaling violation leads to an effective dimension $\tilde{d} = d - \theta$ and therefore in a theory with nonvanishing θ , effective spatial dimension decreases (increases) for larger (smaller) values of hyperscaling violating exponent. Hence for larger values of θ we expect that the spatial correlations between subregions decrease and the resultant E_W decreases.⁸

4 Corner Contributions to EWCS

In this section we study the corner contribution to the EWCS for holographic CFTs dual to Einstein gravity. In the holographic context, considering singular entangling surfaces was first done in [49]. Various features of holographic entanglement entropy for regions with a singular boundary such as cone and crease have been studied, e.g., see [50–53]. A key feature of these studies is the appearance of a new logarithmic term in the HEE which depends on the central charge of the underlying CFT. The coefficient of this universal term depends on the opening angle of the corresponding singular surface such that in the smooth limit where the singularity disappears, vanishes. It is worthwhile to point that, corner contributions to other entanglement/information measures is also studied, e.g., see [54, 55]. In particular, for a specific configuration (see Fig.9) the HMI becomes UV divergent when the singular subregions coincide [54]. In the following considering the same setup, we would like to investigate to what extent these singularities in the boundary of entangling regions modify the behavior of EWCS. To begin with, we will compute EWCS for a union of kinks in $d = 2$ in the next subsection.

⁸We would like to thank Ali Mollabashi for useful comments about this point.

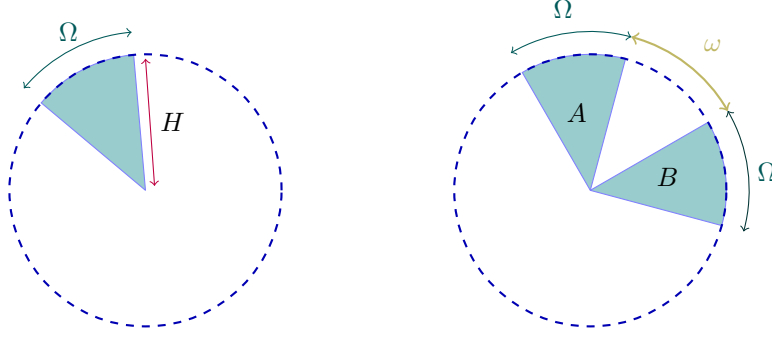


Figure 9: Schematic configuration for computing HEE (left) and EWCS (right) in $d = 2$ when the entangling region contains a corner.

4.1 EWCS for a Union of Kinks in AdS_4

In this section, in order to find the EWCS for a union of kinks, we use the following 4-dimensional bulk geometry

$$ds^2 = \frac{1}{r^2} (-dt^2 + dr^2 + d\rho^2 + \rho^2 d\phi^2), \quad (4.1)$$

where we have written the boundary spatial directions in polar coordinates. A kink entangling region is specified by

$$t = \text{const.}, \quad 0 \leq \rho \leq H, \quad -\Omega \leq 2\phi \leq \Omega, \quad (4.2)$$

where H is the IR cut-off (see Fig.9). Due to the scaling symmetry of the AdS background and the fact that ρ is the only scale in our setup, for the RT surface we choose the parametrization $r(\rho, \phi) = \rho \Phi(\phi)$. In this case the corresponding HEE functional becomes

$$S = \frac{1}{4G_N} \int_{\frac{\epsilon}{\Phi_t}}^H \frac{d\rho}{\rho} \int_0^{\frac{\Omega}{2}-\delta} \frac{d\phi}{\Phi} \sqrt{1 + \Phi^2 + \Phi'^2}, \quad (4.3)$$

where $\Phi_t \equiv \Phi(0)$ is the turning point given by $\Phi'(0) = 0$ and $\epsilon = \rho \Phi(\frac{\Omega}{2} - \delta)$ is the UV cut off. Since there is no explicit ϕ dependence, the corresponding Hamiltonian is a conserved quantity. Therefore, we find the following first integral

$$\frac{1 + \Phi^2}{\Phi^2 \sqrt{1 + \Phi^2 + \Phi'^2}} = \frac{\sqrt{1 + \Phi_t^2}}{\Phi_t^2}. \quad (4.4)$$

Using the above equation and the boundary condition eq.(4.2), the opening angle is

$$\Omega = \int_0^{\Phi_t} d\Phi \frac{\Phi^2 \sqrt{1 + \Phi_t^2}}{\sqrt{1 + \Phi^2} \sqrt{\Phi_t^4 (1 + \Phi^2) - \Phi^4 (1 + \Phi_t^2)}}. \quad (4.5)$$

Substituting eq.(4.4) back into the expression for the HEE eq.(4.3), we finally obtain

$$S(\Omega) = \frac{1}{2G_N} \frac{H}{\epsilon} - s(\Omega) \log \frac{H}{\epsilon} - \frac{\pi}{4G_N \Phi_t} - s(\Omega) \log \Phi_t + \mathcal{O}\left(\frac{\epsilon}{H}\right), \quad (4.6)$$

where

$$s(\Omega) = \frac{1}{2G_N} \int_0^\infty du \left(1 - \frac{\sqrt{1 + \Phi_t^2(1 + u^2)}}{\sqrt{2 + \Phi_t^2(1 + u^2)}} \right). \quad (4.7)$$

The precise expression for the coefficient of the new universal term can be obtained in certain limits. In particular in $\Omega \rightarrow 0$ limit where we have a sharp corner, one finds [49, 51]

$$s(\Omega \rightarrow 0) \sim \frac{\kappa}{\Omega} + \dots, \quad \kappa = \frac{\pi^2}{6} \Gamma\left(\frac{3}{4}\right)^4 C_T, \quad (4.8)$$

where $C_T \equiv \frac{3}{\pi^3 G_N}$ is the central charge appearing in two-point function of the stress tensor for the underlying CFT.⁹ These results are easily extended to general multipartite subregions, to compute other entanglement measures, e.g., mutual and tripartite information (see [54] for a complete discussion).

In order to compute E_W we consider the configuration depicted in the right panel of Fig.9. Once again we focus our attention on the connected configuration for RT surfaces where both the HMI and EWCS are nonzero. Note that due to the axial symmetry we expect that the minimal cross section of entanglement wedge locates at $\phi = 0$. Using eq.(4.1), the EWCS functional is given by

$$E_W = \frac{1}{4G_N} \int_\epsilon^H d\rho \int_{\rho\Phi_t(\omega)}^{\rho\Phi_t(2\Omega+\omega)} \frac{dr}{r^2}, \quad (4.10)$$

where $\Phi_t(\omega)$ and $\Phi_t(2\Omega + \omega)$ denote the turning points of the corresponding minimal surfaces. The above integral can be evaluated explicitly yielding

$$E_W = \frac{1}{4G_N} \left(\frac{1}{\Phi_t(\omega)} - \frac{1}{\Phi_t(2\Omega + \omega)} \right) \log \frac{H}{\epsilon}, \quad (4.11)$$

which demonstrates that EWCS is divergent when the subregions coincide. It is worth to mention that precisely, the similar situation arose in [54] in investigating the structure of HMI, although the transition is continuous. Considering the case where we have two adjacent sharp corners, i.e., $\omega \ll \Omega \ll 1$ and using eq.(4.8) we may further simplify the result to

$$E_W = \frac{\sqrt{\pi/2}}{\Gamma^2(3/4)} \kappa \left(\frac{1}{\omega} - \frac{1}{\Omega} \right) \log \frac{H}{\epsilon} \sim \frac{\sqrt{\pi/2}}{\Gamma^2(3/4)} \frac{\kappa}{\omega} \log \frac{H}{\epsilon}. \quad (4.12)$$

⁹The explicit expression for the corresponding two-point function is

$$\langle T_{\mu\nu}(r) T_{\alpha\beta}(0) \rangle = \frac{C_T}{r^{2d}} \mathcal{I}_{\mu\nu, \alpha\beta}(r), \quad (4.9)$$

where $\mathcal{I}_{\mu\nu, \alpha\beta}$ is a tensor fixed by symmetry.

It is important to mention that the above result can be obtained using a conformal map relating the corner geometry to a strip in four dimensions. A similar derivation to the one presented for HMI in [54] holds in the present case which shows that the above expression reduces to eq.(2.34) for $d = 2$. As another consistency check, we note that the EWCS should satisfy eq.(1.5). Indeed, as shown in [54] the HMI in this particular limit is given by

$$I = \kappa \left(\frac{1}{\omega} - \frac{2}{\Omega} + \frac{1}{2\Omega + \omega} \right) \log \frac{H}{\epsilon} \sim \frac{\kappa}{\omega} \log \frac{H}{\epsilon}. \quad (4.13)$$

In comparing the above expression with eq.(4.12), we see that the constraint on the lower bound of EWCS satisfied.

4.2 EWCS for a Union of Creases in AdS_{d+2}

In this section we will compute the EWCS in the presence of singular regions in higher dimensions. The calculations are analogous to those for three dimensions. Consider the following bulk geometry

$$ds^2 = \frac{1}{r^2} \left(-dt^2 + dr^2 + d\rho^2 + \rho^2 d\phi^2 + \sum_{i=1}^{d-2} dx_i^2 \right). \quad (4.14)$$

In this case the entangling region is specified by

$$t = \text{const.}, \quad 0 \leq \rho \leq H, \quad -\Omega \leq 2\phi \leq \Omega, \quad 0 < x_i < \tilde{H}, \quad (4.15)$$

where H and \tilde{H} are the IR regulators where in the following we set $\tilde{H} = H$. Using the scaling symmetry of the background and assuming $r(\rho, \phi) = \rho \Phi(\phi)$, the corresponding HEE functional becomes

$$S = \frac{H^{d-2}}{4G_N} \int_{\frac{\epsilon}{\Phi_t}}^H \frac{d\rho}{\rho^{d-1}} \int_0^{\frac{\Omega}{2}-\delta} d\phi \frac{\sqrt{1 + \Phi^2 + \Phi'^2}}{\Phi^d}. \quad (4.16)$$

Once again, since there is no explicit ϕ dependence, we have a first integral [50]

$$\mathcal{K}_d \equiv \frac{(1 + \Phi^2)^{\frac{d}{2}}}{\Phi^d \sqrt{1 + \Phi^2 + \Phi'^2}} = \frac{(1 + \Phi_t^2)^{\frac{d-1}{2}}}{\Phi_t^d}. \quad (4.17)$$

This eventually leads to the following expression for the opening angle and HEE

$$\begin{aligned} \Omega &= 2\mathcal{K}_d \int_0^{\Phi_t} d\Phi \frac{\Phi^d}{\sqrt{1 + \Phi^2} \sqrt{(1 + \Phi^2)^{d-1} - \mathcal{K}_d^2 \Phi^{2d}}}, \\ S &= \frac{H^{d-2}}{2G_N} \left(\frac{H}{(d-1)\epsilon^{d-1}} + \frac{\mathcal{F}(\Omega)}{(d-2)\epsilon^{d-2}} \right) + \mathcal{O}(\epsilon), \end{aligned} \quad (4.18)$$

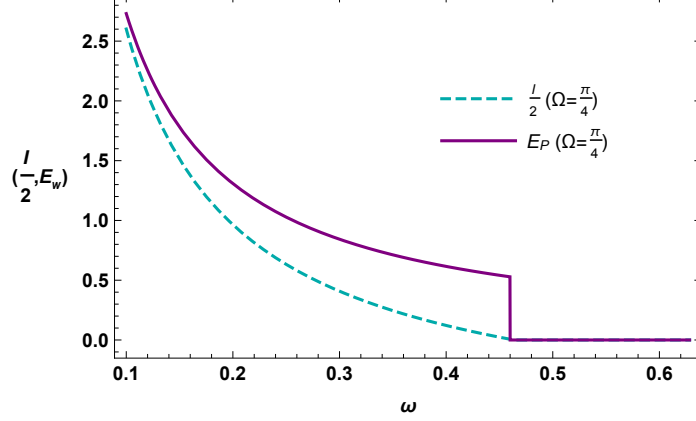


Figure 10: EWCS (HMI) as a function of ω in $d = 3$ that undergoes a discontinuous (continuous) phase transition beyond which it is identically zero. Here we normalize these quantities by a factor of $2G_N\epsilon/H$.

where we have defined

$$\mathcal{F}(\Omega) = -\frac{1}{\Phi_t(\Omega)} - \int_0^{\Phi_t(\Omega)} \frac{d\Phi}{\Phi^2} \left(1 + \frac{\sqrt{1 + \Phi^2 + \Phi'^2}}{\Phi'} \right). \quad (4.19)$$

It is worth to mention that the second divergent term in eq.(4.18) is produced by the singularity in the entangling surface and vanish when the surface is smooth. We would like to stress that this contribution is due to adding a flat locus to the kink [50]. Further in $d = 2$ this term modified and we recover a universal logarithmic contribution.

Turning to EWCS, we expect that the minimal cross section of entanglement wedge locates at $\phi = 0$. Using eq.(4.14), one finds

$$E_W = \frac{H^{d-2}}{4G_N} \int_\epsilon^H d\rho \int_{\rho\Phi_t(\omega)}^{\rho\Phi_t(2\Omega+\omega)} \frac{dr}{r^d} = \frac{H^{d-2}}{4(d-1)G_N} \left(\frac{1}{\Phi_t(\omega)} - \frac{1}{\Phi_t(2\Omega+\omega)} \right) \int_\epsilon^H \frac{d\rho}{\rho^{d-1}}. \quad (4.20)$$

Evaluating the above integral, we are left with

$$E_W = \frac{1}{4(d-1)(d-2)G_N} \left(\frac{1}{\Phi_t(\omega)} - \frac{1}{\Phi_t(2\Omega+\omega)} \right) \frac{H^{d-2}}{\epsilon^{d-2}}, \quad (4.21)$$

which is divergent and obeys the area law. The final result for E_W in various dimensions agree at a qualitative level, so we just consider $d = 3$ case. In Fig.10 we demonstrate the EWCS as a function of ω for $\Omega = \frac{\pi}{4}$. We observe that E_W is a monotonically decreasing function of the angular separation between the two subregions and for distant enough regions $E_W = 0$. Further, as a consistency check in this figure we also plot $\frac{I}{2}$ to see whether eq.(1.5) satisfied or not. Here, it is worth mentioning that, it was shown in [54] that HMI for a union of creases in $\omega \ll \Omega$ limit is

given by the following expression¹⁰

$$I = \frac{1}{2(d-2)G_N} (2\mathcal{F}(\Omega) - \mathcal{F}(2\Omega + \omega) - \mathcal{F}(\omega)) \frac{H^{d-2}}{\epsilon^{d-2}}, \quad (4.22)$$

which is divergent.

5 Conclusions and Discussions

In this paper, we explored the general behavior of entanglement wedge cross section (EWCS) in various geometries and for different entangling regions. Based on different holographic interpretation of E_W , this quantity may be dual to entanglement of purification, logarithmic negativity and reflected entropy [13–15, 17]. In the following we would like to first summarize our main results and then continue with discussing some further problems.

- In a two dimensional relativistic quantum field theory E_W is a monotonically decreasing function of temperature such that at higher temperature the two subsystems becomes more disentangled. Also keeping the length and separation of the subregions fixed while temperature increases, the E_W shows a discontinuous phase transition, such that $E_W = 0$ when T is high enough. In the bulk, the vanishing of E_W results because of the disconnected configuration for the RT surfaces and the fact that in this case the corresponding entanglement wedge is disconnected, e.g., see Fig.2.
- In higher dimensions considering a strip entangling region, the qualitative behaviors of E_W at finite temperature are very similar to $d = 1$ case. A key observation is that the E_W obeys an area law even in finite temperature where the HEE shows a volume law. Therefore one may regard the E_W as a more appropriate measure of quantum correlations for thermal mixed states.¹¹
- In a nonrelativistic field theory with nontrivial dynamical and hyperscaling exponents, E_W is a monotonically decreasing function of temperature and the separation between subregions. In this case the transition point after that E_W vanishes, depends on the value of z and θ . In particular E_W is an increasing function of the dynamical exponent and the transition which happens in large separation or high temperature limit is slower in comparing to the relativistic case with $z = 1$. As we mentioned, the physical reason behind this is that the quantum correlations between subregions increase as one increases z . On the other hand, E_W is monotonically decreasing as the hyperscaling violating exponent increases. In a field theory with nonvanishing θ , effective spatial dimension, i.e, $\tilde{d} = d - \theta$, decreases for larger values of

¹⁰Note that in $\Omega \ll \omega$ limit the HMI vanishes.

¹¹It is important to mention that regarding other basic properties of correlation measures for mixed states and the holographic interpretation of E_W in terms of EoP, the EoP fails to be an ideal measure of entanglement, because it is not monotonically decreasing under LOCC.

hyperscaling violating exponent and therefore for larger values of θ we expect that the spatial correlations between subregions decrease and the resultant E_W decreases.

- Considering an entangling region with singular boundary, we demonstrated that E_W is divergent when the subregions coincide. In particular for a three dimensional boundary theory we found a universal contribution to E_W due to the presence of corner where the coefficient is proportional to the central charge for the underlying CFT. Moreover, considering a singular region in higher dimensions we verified that the corresponding E_W obeys area law.

We can extend this study to different interesting directions. A key feature of E_W is the discontinuous phase transition which happens at large separation or high temperature. As we mentioned before, the corresponding (continuous) phase transition of HMI is a reminiscent of the large N limit of the dual field theory and it disappears if one considers quantum corrections. It will be an important future problem to study the quantum corrections to E_W using the prescription proposed in [8]. We expect that considering this quantum corrections change the phase diagram of E_W and especially one find a smooth behavior near the critical point.

Finally it would be interesting to study E_W in more general holographic setups, e.g., higher curvature gravities. It is known that for such theories the RT prescription for computing HEE fails and one should use other proposals [3–6]. At present, our preliminary analysis suggests that in this case one should replace eq.(1.3) with another functional which contains higher curvature corrections. We leave the details of this interesting problem for future study [56].

Acknowledgements

We are very grateful to Mohsen Alishahiha and Ali Mollabashi for correspondence, careful reading of the manuscript and their valuable comments.

A Thermal Corrections to HEE and HMI in Nonrelativistic Theories

In this appendix we briefly review the low and high temperature expansions of HEE and HMI in nonrelativistic theories with Lifshitz and hyperscaling violating exponents. Here we only focus on the main steps and for further discussions we refer to [34].

Similar to section 2.1 we consider a strip entangling region (see Fig. 3) for computing HEE and HMI and parametrize the corresponding hypersurface as eq.(2.3). Employing the RT prescription and using eq.(3.2), the corresponding HEE functional is given by

$$S = \frac{H^{d-1}}{4G_N} \int \frac{dr}{r^{\tilde{d}}} \sqrt{\frac{1}{f(r)} + x'(r)^2}, \quad (\text{A.1})$$

where we have defined an effective dimension $\tilde{d} = d - \theta$. Extremizing this functional yields the

equation of motion for $x(r)$

$$x'(r) = \pm \frac{1}{\sqrt{f(r) \left(\left(\frac{r_t}{r} \right)^{2\tilde{d}} - 1 \right)}}, \quad (\text{A.2})$$

where r_t denotes the turning point of the minimal hypersurface. Now we can obtain the relation between ℓ and r_t as

$$\ell = 2r_t \int_0^1 \frac{u^{\tilde{d}} du}{\sqrt{1 - u^{2\tilde{d}}}} \left(1 - \left(\frac{r_t}{r_0} \right)^{\tilde{d}+z} u^{\tilde{d}+z} \right)^{-\frac{1}{2}}. \quad (\text{A.3})$$

In addition, the HEE is given by on-shell functional of eq.(A.1) for the hypersurface eq.(A.2)

$$S = \frac{1}{2G_N} \frac{H^{d-1}}{r_t^{\tilde{d}-1}} \int_{\frac{\epsilon}{r_t}}^1 \frac{du u^{-\tilde{d}}}{\sqrt{1 - u^{2\tilde{d}}}} \left(1 - \left(\frac{r_t}{r_0} \right)^{\tilde{d}+z} u^{\tilde{d}+z} \right)^{-\frac{1}{2}}. \quad (\text{A.4})$$

One may consider two special cases $d = \theta$ and $\theta = d - 1$, $z = 1$. In the former, the RT surface lies on the boundary slice $r = \epsilon$ and we have an extensive violation of area law [39]. The latter, up to an overall factor H^θ , is exactly same as $d = 1$ relativistic theory so we do not mention it again (see section 2.1.1). Therefore, in the rest, we neglect these two special cases.

By employing method of section 2 we can extract the behavior of HEE and HMI at low and high temperature. Using binomial series and performing the integral we obtain the relation between length of entangling region ℓ and turning point r_t as

$$\ell = 2r_t \sum_{n=0}^{\infty} \frac{1}{1 + n(\tilde{d} + z)} \frac{\Gamma(n + \frac{1}{2})}{\Gamma(n + 1)} \frac{\Gamma\left(\frac{\tilde{d}+1+n(\tilde{d}+z)}{2\tilde{d}}\right)}{\Gamma\left(\frac{(\tilde{d}+z)n+1}{2\tilde{d}}\right)} \left(\frac{r_t}{r_0} \right)^{n(\tilde{d}+z)}, \quad (\text{A.5})$$

This series converges for $r_t < r_0$ when $\tilde{d} + z > 0$. A similar calculation for HEE functional eq.(A.4) shows that

$$S = \frac{1}{2G_N(\tilde{d} - 1)} \frac{H^{d-1}}{e^{\tilde{d}-1}} + S_{\text{finite}}, \quad (\text{A.6})$$

where

$$S_{\text{finite}} = \frac{1}{4G_N} \frac{H^{d-1}}{r_t^{\tilde{d}-1}} \left(\frac{\tilde{c}}{1 - \tilde{d}} + \sum_{n=1}^{\infty} \frac{1}{\tilde{d}} \frac{\Gamma(n + \frac{1}{2})}{\Gamma(n + 1)} \frac{\Gamma\left(\frac{n(\tilde{d}+z) - \tilde{d} + 1}{2\tilde{d}}\right)}{\Gamma\left(\frac{n(\tilde{d}+z) + 1}{2\tilde{d}}\right)} \left(\frac{r_t}{r_0} \right)^{n(\tilde{d}+z)} \right), \quad (\text{A.7})$$

and we have define $\tilde{c} = \frac{2\sqrt{\pi}\Gamma\left(\frac{\tilde{d}+1}{2\tilde{d}}\right)}{\Gamma\left(\frac{1}{2\tilde{d}}\right)}$. Using these results we can find the low and high temperature behavior of HEE and HMI.

(i) HEE at Low Temperature Limit $\ell T^{\frac{1}{z}} \ll 1$

By using eq.(3.4) the $\ell T^{\frac{1}{z}} \ll 1$ limit can be interpreted as $r_t \ll r_0$. In this limit we can solve eq.(2.14) for r_t

$$r_t = \frac{\ell}{\tilde{c}} \left(1 - \frac{\sqrt{\pi}}{(\tilde{d} + z + 1)\tilde{c}^{\tilde{d}+z+1}} \frac{\Gamma\left(\frac{2\tilde{d}+z+1}{2\tilde{d}}\right)}{\Gamma\left(\frac{\tilde{d}+z+1}{2\tilde{d}}\right)} \left(\frac{\ell}{r_0}\right)^{\tilde{d}+z} + \mathcal{O}\left(\left(\frac{\ell}{r_0}\right)^{2(\tilde{d}+z)}\right) \right). \quad (\text{A.8})$$

Plugging r_t into eq.(A.7) and using eq.(3.4), the low temperature corrections to finite part of HEE obtains

$$S_{\text{finite.}} = \frac{\tilde{C}_0}{4G_N} \frac{H^{d-1}}{\ell^{d-1}} \left(1 + \tilde{C}_1 (\ell T^{\frac{1}{z}})^{\tilde{d}+z} + \mathcal{O}((\ell T)^{2(\tilde{d}+z)}) \right), \quad (\text{A.9})$$

where

$$\tilde{C}_0 = \frac{\tilde{c}^{\tilde{d}}}{1 - \tilde{d}}, \quad \tilde{C}_1 = \left(\frac{4\pi}{|\tilde{d} + z|} \right)^{\frac{\tilde{d}+z}{z}} \frac{\sqrt{\pi}}{2\tilde{c}^{\tilde{d}+z+1}} \frac{1 - \tilde{d}}{\tilde{d} + z + 1} \frac{\Gamma\left(\frac{z+1}{2\tilde{d}}\right)}{\Gamma\left(\frac{\tilde{d}+z+1}{2\tilde{d}}\right)}. \quad (\text{A.10})$$

For $z > -1 - \tilde{d}$ the thermal correction increases the HEE. However, for $z < -1 - \tilde{d}$ the HEE decreases by thermal correction, but as we mentioned, the negative value of z (for $\theta > d$) has been excluded by thermodynamic stability of black brane solution.

(ii) HEE at High Temperature Limit $\ell T \gg 1$

In the high temperature the near horizon part of RT surface has the main contribution to HEE. Therefore, to obtain HEE we can consider eqs.(A.5) and (A.7) in the limit that $r_t \rightarrow r_0$. By manipulating eq.(A.7) we get

$$S_{\text{finite}} = \frac{H^{d-1}}{4G_N r_t^{\tilde{d}-1}} \left(\frac{\ell}{r_t} - \frac{\tilde{c}\tilde{d}}{\tilde{d}-1} + \sum_{n=1}^{\infty} \frac{1}{2\tilde{d}} \frac{\Gamma\left(n + \frac{1}{2}\right)}{\Gamma(n+1)} \frac{\Gamma\left(\frac{n(\tilde{d}+z)-\tilde{d}+1}{2\tilde{d}}\right)}{\Gamma\left(\frac{n(\tilde{d}+z)+2\tilde{d}+1}{2\tilde{d}}\right)} \left(\frac{r_t}{r_0}\right)^{n(\tilde{d}+z)} \right).$$

In the large n limit the above series behaves as $\frac{1}{n^z} \left(\frac{r_t}{r_0}\right)^{n\tilde{d}+z}$, so we can take $r_t \rightarrow r_0$ limit. Now using eq.(3.4), we obtain the finite part of HEE at high temperature

$$S_{\text{finite}} = \frac{\ell H^{d-1}}{4G_N} \left(\frac{4\pi T}{|\tilde{d} + z|} \right)^{\frac{\tilde{d}}{z}} \left(1 + \left(\frac{|\tilde{d} + z|}{4\pi \ell^z T} \right)^{\frac{1}{z}} \tilde{C}_2 \right), \quad (\text{A.11})$$

where

$$\tilde{\mathcal{C}}_2 = -\frac{\tilde{c}\tilde{d}}{\tilde{d}-1} + \sum_{n=1}^{\infty} \frac{1}{2\tilde{d}} \frac{\Gamma(n+\frac{1}{2})}{\Gamma(n+1)} \frac{\Gamma\left(\frac{n(\tilde{d}+z)-\tilde{d}+1}{2\tilde{d}}\right)}{\Gamma\left(\frac{n(\tilde{d}+z)+2\tilde{d}+1}{2\tilde{d}}\right)}. \quad (\text{A.12})$$

(iii) HMI at Low and High Temperature Limit

Now we are ready to obtain the HMI for the configuration depicted in Fig. 3 using eqs.(A.9) and (A.11). We only consider cases where the HMI is non-zero corresponding to a connected configuration. In this case using eq.(2.22) for eq.(A.9) and assuming $hT^{\frac{1}{z}} \ll \ell T^{\frac{1}{z}} \ll 1$ we get the HMI

$$I = I_{T=0} - \tilde{\mathcal{C}}_0 \tilde{\mathcal{C}}_1 \frac{H^{d-1}}{2G_N} T^{\frac{\tilde{d}+z}{z}} \left((h+2\ell)^{z+1} - 2\ell^{z+1} + h^{z+1} \right), \quad (\text{A.13})$$

where $I_{T=0}$ is the HMI at zero temperature

$$I_{T=0} = \tilde{\mathcal{C}}_0 \frac{H^{d-1}}{4G_N} \left(\frac{2}{\ell^{\tilde{d}-1}} - \frac{1}{h^{\tilde{d}-1}} - \frac{1}{(2\ell+h)^{\tilde{d}-1}} \right). \quad (\text{A.14})$$

Note that the subadditivity implies $\tilde{\mathcal{C}}_0 < 0$ which happens for $\tilde{d} > 1$. In addition, it shows that the thermal fluctuation decreases HMI.

Finally using eqs.(A.11) and (A.9) for $hT^{\frac{1}{z}} \ll 1 \ll \ell T^{\frac{1}{z}}$ we can find the high temperature behavior of HMI as

$$I = \frac{H^{d-1} T^{\frac{\tilde{d}-1}{z}}}{4G_N} \left(-\frac{\tilde{\mathcal{C}}_0}{(hT^{\frac{1}{z}})^{\tilde{d}-1}} + \left(\frac{4\pi}{|\tilde{d}+z|} \right)^{\frac{\tilde{d}-1}{z}} \tilde{\mathcal{C}}_2 - \left(\frac{4\pi}{|\tilde{d}+z|} \right)^{\frac{\tilde{d}}{z}} hT^{\frac{1}{z}} - \tilde{\mathcal{C}}_0 \tilde{\mathcal{C}}_1 (hT^{\frac{1}{z}})^{z+1} \right). \quad (\text{A.15})$$

References

- [1] S. Ryu and T. Takayanagi, ‘‘Holographic derivation of entanglement entropy from AdS/CFT,’’ *Phys. Rev. Lett.* **96**, 181602 (2006) [[hep-th/0603001](#)].
- [2] V. E. Hubeny, M. Rangamani and T. Takayanagi, ‘‘A Covariant holographic entanglement entropy proposal,’’ *JHEP* **0707**, 062 (2007) doi:10.1088/1126-6708/2007/07/062 [[arXiv:0705.0016](#) [hep-th]].
- [3] L. Y. Hung, R. C. Myers and M. Smolkin, ‘‘On Holographic Entanglement Entropy and Higher Curvature Gravity,’’ *JHEP* **1104**, 025 (2011) doi:10.1007/JHEP04(2011)025 [[arXiv:1101.5813](#) [hep-th]].
- [4] X. Dong, ‘‘Holographic Entanglement Entropy for General Higher Derivative Gravity,’’ *JHEP* **1401**, 044 (2014) doi:10.1007/JHEP01(2014)044 [[arXiv:1310.5713](#) [hep-th]].

- [5] J. Camps, “Generalized entropy and higher derivative Gravity,” *JHEP* **1403**, 070 (2014) doi:10.1007/JHEP03(2014)070 [[arXiv:1310.6659](#) [hep-th]].
- [6] M. R. Mohammadi Mozaffar, A. Mollabashi, M. M. Sheikh-Jabbari and M. H. Vahidinia, “Holographic Entanglement Entropy, Field Redefinition Invariance and Higher Derivative Gravity Theories,” *Phys. Rev. D* **94**, no. 4, 046002 (2016) doi:10.1103/PhysRevD.94.046002 [[arXiv:1603.05713](#) [hep-th]].
- [7] M. Headrick, “Entanglement Renyi entropies in holographic theories,” *Phys. Rev. D* **82**, 126010 (2010) [[arXiv:1006.0047](#) [hep-th]].
- [8] T. Faulkner, A. Lewkowycz and J. Maldacena, “Quantum corrections to holographic entanglement entropy,” *JHEP* **1311**, 074 (2013) doi:10.1007/JHEP11(2013)074 [[arXiv:1307.2892](#) [hep-th]].
- [9] D. L. Jafferis, A. Lewkowycz, J. Maldacena and S. J. Suh, “Relative entropy equals bulk relative entropy,” *JHEP* **1606**, 004 (2016) doi:10.1007/JHEP06(2016)004 [[arXiv:1512.06431](#) [hep-th]].
- [10] M. Miyaji, T. Numasawa, N. Shiba, T. Takayanagi and K. Watanabe, “Distance between Quantum States and Gauge-Gravity Duality,” *Phys. Rev. Lett.* **115**, no. 26, 261602 (2015) doi:10.1103/PhysRevLett.115.261602 [[arXiv:1507.07555](#) [hep-th]].
- [11] L. Susskind, “Computational Complexity and Black Hole Horizons,” [*Fortsch. Phys.* **64**, 24 (2016)] Addendum: *Fortsch. Phys.* **64**, 44 (2016) doi:10.1002/prop.201500093, 10.1002/prop.201500092 [[arXiv:1403.5695](#) [hep-th], [arXiv:1402.5674](#) [hep-th]].
- [12] A. R. Brown, D. A. Roberts, L. Susskind, B. Swingle and Y. Zhao, “Holographic Complexity Equals Bulk Action?,” *Phys. Rev. Lett.* **116**, no. 19, 191301 (2016) doi:10.1103/PhysRevLett.116.191301 [[arXiv:1509.07876](#) [hep-th]].
- [13] K. Umemoto and T. Takayanagi, “Entanglement of purification through holographic duality,” *Nature Phys.* **14**, no. 6, 573 (2018) doi:10.1038/s41567-018-0075-2 [[arXiv:1708.09393](#) [hep-th]].
- [14] P. Nguyen, T. Devakul, M. G. Halbasch, M. P. Zaletel and B. Swingle, “Entanglement of purification: from spin chains to holography,” *JHEP* **1801**, 098 (2018) doi:10.1007/JHEP01(2018)098 [[arXiv:1709.07424](#) [hep-th]].
- [15] J. Kudler-Flam and S. Ryu, “Entanglement negativity and minimal entanglement wedge cross sections in holographic theories,” [arXiv:1808.00446](#) [hep-th].
- [16] K. Tamaoka, “Entanglement Wedge Cross Section from the Dual Density Matrix,” [arXiv:1809.09109](#) [hep-th].
- [17] S. Dutta and T. Faulkner, “A canonical purification for the entanglement wedge cross-section,” [arXiv:1905.00577](#) [hep-th].

- [18] B. M. Terhal, M. Horodecki, D. W. Leung and D. P. Di- Vincenzo, “The entanglement of purification,” *J. Math. Phys.* **43** (2002) 4286, [arXiv:quant-ph/0202044](#).
- [19] S. Bagchi and A. K. Pati, “Monogamy, polygamy, and other properties of entanglement of purification,” *Phys. Rev. A* **91**, 042323 (2015), [arXiv:1502.01272](#) [quant-ph].
- [20] A. Bhattacharyya, T. Takayanagi and K. Umemoto, “Entanglement of Purification in Free Scalar Field Theories,” *JHEP* **1804**, 132 (2018) doi:10.1007/JHEP04(2018)132 [[arXiv:1802.09545](#) [hep-th]].
- [21] R. Q. Yang, C. Y. Zhang and W. M. Li, “Holographic entanglement of purification for thermofield double states and thermal quench,” *JHEP* **1901**, 114 (2019) doi:10.1007/JHEP01(2019)114 [[arXiv:1810.00420](#) [hep-th]].
- [22] N. Bao and I. F. Halpern, “Holographic Inequalities and Entanglement of Purification,” *JHEP* **1803**, 006 (2018) doi:10.1007/JHEP03(2018)006 [[arXiv:1710.07643](#) [hep-th]].
- [23] H. Hirai, K. Tamaoka and T. Yokoya, “Towards Entanglement of Purification for Conformal Field Theories,” *PTEP* **2018**, no. 6, 063B03 (2018) doi:10.1093/ptep/pty063 [[arXiv:1803.10539](#) [hep-th]].
- [24] R. Espndola, A. Guijosa and J. F. Pedraza, “Entanglement Wedge Reconstruction and Entanglement of Purification,” *Eur. Phys. J. C* **78**, no. 8, 646 (2018) doi:10.1140/epjc/s10052-018-6140-2 [[arXiv:1804.05855](#) [hep-th]].
- [25] N. Bao and I. F. Halpern, “Conditional and Multipartite Entanglements of Purification and Holography,” *Phys. Rev. D* **99**, no. 4, 046010 (2019) doi:10.1103/PhysRevD.99.046010 [[arXiv:1805.00476](#) [hep-th]].
- [26] K. Umemoto and Y. Zhou, “Entanglement of Purification for Multipartite States and its Holographic Dual,” *JHEP* **1810**, 152 (2018) doi:10.1007/JHEP10(2018)152 [[arXiv:1805.02625](#) [hep-th]].
- [27] N. Bao, A. Chatwin-Davies and G. N. Remmen, “Entanglement of Purification and Multi-boundary Wormhole Geometries,” *JHEP* **1902**, 110 (2019) doi:10.1007/JHEP02(2019)110 [[arXiv:1811.01983](#) [hep-th]].
- [28] C. A. Agn, J. De Boer and J. F. Pedraza, “Geometric Aspects of Holographic Bit Threads,” [arXiv:1811.08879](#) [hep-th].
- [29] P. Caputa, M. Miyaji, T. Takayanagi and K. Umemoto, “Holographic Entanglement of Purification from Conformal Field Theories,” [arXiv:1812.05268](#) [hep-th].
- [30] P. Liu, Y. Ling, C. Niu and J. P. Wu, “Entanglement of Purification in Holographic Systems,” [arXiv:1902.02243](#) [hep-th].

- [31] A. Bhattacharyya, A. Jahn, T. Takayanagi and K. Umemoto, “Entanglement of Purification in Many Body Systems and Symmetry Breaking,” [arXiv:1902.02369](#) [hep-th].
- [32] M. Ghodrati, X. M. Kuang, B. Wang, C. Y. Zhang and Y. T. Zhou, “The connection between holographic entanglement and complexity of purification,” [arXiv:1902.02475](#) [hep-th].
- [33] W. Fischler and S. Kundu, “Strongly Coupled Gauge Theories: High and Low Temperature Behavior of Non-local Observables,” *JHEP* **1305**, 098 (2013) doi:10.1007/JHEP05(2013)098 [[arXiv:1212.2643](#) [hep-th]].
- [34] W. Fischler, A. Kundu and S. Kundu, “Holographic Mutual Information at Finite Temperature,” *Phys. Rev. D* **87**, no. 12, 126012 (2013) doi:10.1103/PhysRevD.87.126012 [[arXiv:1212.4764](#) [hep-th]].
- [35] J. Cardy and C. P. Herzog, “Universal Thermal Corrections to Single Interval Entanglement Entropy for Two Dimensional Conformal Field Theories,” *Phys. Rev. Lett.* **112**, no. 17, 171603 (2014) doi:10.1103/PhysRevLett.112.171603 [[arXiv:1403.0578](#) [hep-th]].
- [36] C. P. Herzog, “Universal Thermal Corrections to Entanglement Entropy for Conformal Field Theories on Spheres,” *JHEP* **1410**, 28 (2014) doi:10.1007/JHEP10(2014)028 [[arXiv:1407.1358](#) [hep-th]].
- [37] S. Ryu and T. Takayanagi, “Aspects of Holographic Entanglement Entropy,” *JHEP* **0608**, 045 (2006) doi:10.1088/1126-6708/2006/08/045 [[hep-th/0605073](#)].
- [38] M. Alishahiha, M. R. Mohammadi Mozaffar and M. R. Tanhayi, “On the Time Evolution of Holographic n-partite Information,” *JHEP* **1509**, 165 (2015) doi:10.1007/JHEP09(2015)165 [[arXiv:1406.7677](#) [hep-th]].
- [39] X. Dong, S. Harrison, S. Kachru, G. Torroba and H. Wang, “Aspects of holography for theories with hyperscaling violation,” *JHEP* **1206**, 041 (2012) doi:10.1007/JHEP06(2012)041 [[arXiv:1201.1905](#) [hep-th]].
- [40] M. Alishahiha, E. O. Colgain and H. Yavartanoo, “Charged Black Branes with Hyperscaling Violating Factor,” *JHEP* **1211**, 137 (2012) doi:10.1007/JHEP11(2012)137 [[arXiv:1209.3946](#) [hep-th]].
- [41] J. Gath, J. Hartong, R. Monteiro and N. A. Obers, “Holographic Models for Theories with Hyperscaling Violation,” *JHEP* **1304**, 159 (2013) doi:10.1007/JHEP04(2013)159 [[arXiv:1212.3263](#) [hep-th]].
- [42] M. Alishahiha, A. Faraji Astaneh and M. R. Mohammadi Mozaffar, “Thermalization in backgrounds with hyperscaling violating factor,” *Phys. Rev. D* **90**, no. 4, 046004 (2014) doi:10.1103/PhysRevD.90.046004 [[arXiv:1401.2807](#) [hep-th]].

- [43] M. R. Tanhayi, “Thermalization of Mutual Information in Hyperscaling Violating Backgrounds,” JHEP **1603**, 202 (2016) doi:10.1007/JHEP03(2016)202 [[arXiv:1512.04104](#) [hep-th]].
- [44] M. Alishahiha, A. Faraji Astaneh, M. R. Mohammadi Mozaffar and A. Mollabashi, “Complexity Growth with Lifshitz Scaling and Hyprscaling Violation,” JHEP **1807**, 042 (2018) doi:10.1007/JHEP07(2018)042 [[arXiv:1802.06740](#) [hep-th]].
- [45] M. R. Mohammadi Mozaffar and A. Mollabashi, “Entanglement in Lifshitz-type Quantum Field Theories,” JHEP **1707**, 120 (2017) doi:10.1007/JHEP07(2017)120 [[arXiv:1705.00483](#) [hep-th]].
- [46] T. He, J. M. Magan and S. Vandoren, “Entanglement Entropy in Lifshitz Theories,” SciPost Phys. **3**, no. 5, 034 (2017) doi:10.21468/SciPostPhys.3.5.034 [[arXiv:1705.01147](#) [hep-th]].
- [47] M. R. Mohammadi Mozaffar and A. Mollabashi, “Logarithmic Negativity in Lifshitz Harmonic Models,” J. Stat. Mech. **1805**, no. 5, 053113 (2018) doi:10.1088/1742-5468/aac135 [[arXiv:1712.03731](#) [hep-th]].
- [48] M. R. Mohammadi Mozaffar and A. Mollabashi, “Entanglement Evolution in Lifshitz-type Scalar Theories,” JHEP **1901**, 137 (2019) doi:10.1007/JHEP01(2019)137 [[arXiv:1811.11470](#) [hep-th]].
- [49] T. Hirata and T. Takayanagi, “AdS/CFT and strong subadditivity of entanglement entropy,” JHEP **0702**, 042 (2007) doi:10.1088/1126-6708/2007/02/042 [[hep-th/0608213](#)].
- [50] R. C. Myers and A. Singh, “Entanglement Entropy for Singular Surfaces,” JHEP **1209**, 013 (2012) [[arXiv:1206.5225](#) [hep-th]].
- [51] P. Bueno, R. C. Myers and W. Witczak-Krempa, “Universality of corner entanglement in conformal field theories,” Phys. Rev. Lett. **115**, no. 2, 021602 (2015) [[arXiv:1505.04804](#) [hep-th]].
- [52] M. Alishahiha, A. F. Astaneh, P. Fonda and F. Omidi, “Entanglement Entropy for Singular Surfaces in Hyperscaling violating Theories,” [arXiv:1507.05897](#) [hep-th].
- [53] D. Seminara, J. Sisti and E. Tonni, “Corner contributions to holographic entanglement entropy in AdS₄/BCFT₃,” JHEP **1711**, 076 (2017) doi:10.1007/JHEP11(2017)076 [[arXiv:1708.05080](#) [hep-th]].
- [54] M. R. Mohammadi Mozaffar, A. Mollabashi and F. Omidi, “Holographic Mutual Information for Singular Surfaces,” JHEP **1512**, 082 (2015) doi:10.1007/JHEP12(2015)082 [[arXiv:1511.00244](#) [hep-th]].
- [55] E. Bakhshaei, A. Mollabashi and A. Shirzad, “Holographic Subregion Complexity for Singular Surfaces,” Eur. Phys. J. C **77**, no. 10, 665 (2017) doi:10.1140/epjc/s10052-017-5247-1 [[arXiv:1703.03469](#) [hep-th]].
- [56] Komeil Babaei Velni, M. Reza Mohammadi Mozaffar, M. H. Vahidinia *work in progress*.